

## Influence of Large-Scale Advective Cooling and Moistening Effects on the Quasi-Equilibrium Behavior of Explicitly Simulated Cumulus Ensembles

KUAN-MAN XU AND DAVID A. RANDALL

*Department of Atmospheric Science, Colorado State University, Fort Collins, Colorado*

(Manuscript received 20 January 1997, in final form 5 August 1997)

### ABSTRACT

The influence of large-scale advective cooling and/or moistening on the quasi-equilibrium behavior of simulated, tropical oceanic cumulus ensembles is examined in this study. Two sensitivity simulations are performed by imposing time varying/invariant large-scale advective cooling effects and time invariant/varying large-scale advective moistening effects. The results are compared with a control simulation performed with both large-scale advective cooling and moistening effects that are time varying.

It is found that the generalized convective available potential energy (GCAPE) tendency is almost one order of magnitude smaller than the GCAPE production in all simulations. This indicates that the quasi-equilibrium assumption of Arakawa and Schubert is well justified. The higher-order behavior of quasi-equilibrium cumulus ensemble is then examined. It is found that the GCAPE variations are nearly equally contributed by temperature and water vapor variations in the control simulation. In the sensitivity simulations, they are mainly contributed by the temperature (water vapor) variations even though the imposed large-scale advective cooling (moistening) is time invariant. A significant finding of this study is that there is a negative lag correlation between GCAPE and the intensity of cumulus convection. The lag corresponding to the largest negative correlation ranges from 1 to 5 h in various simulations. The existence of a negative correlation and the maximum lag of a few hours is independent of the character and period of the imposed large-scale advective forcing. The maximum lag can be interpreted as the adjustment timescale from disequilibrium to quasi-equilibrium states in the presence of time-varying large-scale forcing.

### 1. Introduction

The roles of cumulus convection on influencing the behavior of large-scale circulations are well known. For example, cumulus convection transports moisture, momentum, and energy; releases latent heat; and produces precipitation (e.g., Riehl and Malkus 1958). The effects of cumulus convection on large-scale circulations operate on small horizontal scales and thus cannot be resolved with the conventional grid size ( $\sim 500$  km) of large-scale models. Therefore, the collective effects of subgrid-scale cloud processes have to be parameterized in terms of the prognostic variables of resolvable scale. This is the problem of cloud parameterization, which includes formulations of i) convective-scale transports, ii) stratiform precipitation, and iii) cloud-radiation interactions. A quantitative understanding of the basic physical processes and macroscopic behavior of cloud ensembles is essential in order to address this problem.

One of the key issues in understanding the basic physical processes of cumulus convection is what controls/

regulates the intensity of cumulus convection. One of the earliest views is that moisture convergence causes cumulus convection. This was based on the observations that deep convection over the tropical oceans is always accompanied by synoptic-scale convergence at low levels. This view was elevated into the theory of CISK (conditional instability of the second kind) for hurricane development whereby large-scale and convective-scale circulations cooperate (Charney and Eliassen 1964). It was later incorporated into the Kuo cumulus parameterization (Kuo 1965, 1974), which assumed that the amount of convection is related to the total column-integrated moisture convergence. As recently argued by Raymond (1995), such an observed relationship does not necessarily imply that the intensity of cumulus convection is controlled by the large-scale convergence. Based on the mass balance, the temporal fluctuations in convective mass flux and large-scale convergence are well correlated regardless of the ultimate cause of cumulus convection because the clear-air subsidence does not fluctuate much.

An alternative view was established in terms of the convective instability, that is, an assumption on the approximate balance between the generation of convective instability by large-scale processes and its destruction due to cumulus convection itself (Manabe and Strickler

---

*Corresponding author address:* Dr. Kuan-Man Xu, Department of Atmospheric Science, Colorado State University, Fort Collins, CO 80523.  
E-mail: kmxu@atmos.colostate.edu.

1964; Arakawa 1969; Arakawa and Schubert 1974; Lord and Arakawa 1980). If the timescale of large-scale processes is significantly greater than the adjustment timescale, which is the time required for convective-scale processes to reduce convective instability to zero in the absence of large-scale forcing, then the intensity of cumulus convection is controlled by the rate of generation of convective instability due to large-scale processes. This balance does not explicitly determine the quasi-equilibrium state. Instead, it puts a constraint on both temperature and water vapor mixing ratio profiles so that convective instability is minimized (Arakawa and Schubert 1974; Arakawa and Chen 1987).

A third, although relatively new, view is the boundary-layer equilibrium proposed by Raymond (1995), who ignored everything except the boundary layer. It differs from quasi-equilibrium thinking in that the convective available potential energy (CAPE) of a surface parcel rising through the free troposphere no longer enters directly into the equilibrium process. Such an equilibrium is controlled by the balance between surface enthalpy fluxes and input of low-enthalpy air into the subcloud layer (SCL) by convective downdrafts. Raymond (1995) further argued that cumulus convection is typically controlled by the buoyancy difference between the boundary layer parcel and the environmental air just above the boundary layer. Although there is some observational evidence from the TOGA COARE (Tropical Oceans Global Atmosphere Coupled Ocean-Atmosphere Response Experiment; Webster and Lukas 1992), the observations are not used by Raymond (1995) to demonstrate such a balance for an ensemble of clouds over a large-scale domain. Instead, the arguments are based upon the behavior of individual clouds and their SCL properties.

The present study is aimed at further understanding the quasi-equilibrium behavior of cumulus convection by examining the relationship between CAPE and the intensity of cumulus convection and by exploring the relative importance of large-scale thermal destabilization and moisture convergence.

The existence of quasi equilibrium between convective-scale and large-scale processes has been extensively examined with observational and numerically simulated datasets (e.g., Lord and Arakawa 1980; Grell et al. 1991; Xu and Arakawa 1992). Such a quasi equilibrium does allow that convective instability of the atmosphere, which is a function of the lapse rate and the available moisture, changes with time as long as its rate of change is much smaller than the rate of generation by large-scale processes. In fact, observations showed that convective instability varies with time (e.g., Thompson et al. 1979; Williams and Renno 1993; Stevens et al. 1997). Such variations can have an impact on the intensity of cumulus convection. The relationship between the intensity of cumulus convection and the convective instability is termed as the higher-order behavior of cumulus ensembles in this study.

Observations from the GARP (Global Atmospheric Research Program) Atlantic Tropical Experiment (GATE; Kuettner and Parker 1976) indicated that there is a negative correlation between CAPE and the radar-observed surface precipitation rate for composited easterly waves (Thompson et al. 1979). Cheng and Yanai (1989) and Wang and Randall (1994) showed that CAPE accumulates before cumulus convection begins during GATE Phase III and that CAPE reaches its minimum after the time of maximum surface precipitation. Cheng and Yanai (1989) attributed this phase relationship to the coupling between thermodynamic and dynamic fields in the environment of organized cumulus convection. This phase relationship provides direct evidence that the adjustment timescale is finite. Then, how long is the *adjustment timescale* under different large-scale *advective processes*? The answer to this question is important because there has been a trend to relax the quasi-equilibrium assumption in cumulus parameterizations (e.g., Betts and Miller 1986; Emanuel 1991; Moorthi and Suarez 1992; Randall and Pan 1993). Because of the coarse temporal resolutions of the observational datasets (e.g., 3 h for GATE and 6 h for TOGA COARE), such a question can only be addressed with a modeling approach using a cloud ensemble model (CEM) that explicitly resolves individual clouds but covers a large horizontal area.

Another issue of considerable debate is the relative importance of large-scale thermal destabilization and moisture convergence in forcing convection (e.g., Kuo 1965, 1974; Arakawa and Schubert 1974; Xu and Arakawa 1992) because both tend to increase the convective instability. In nature, convection is simultaneously forced by both thermal destabilization and moisture convergence so that it is difficult to separate their effects. Therefore, using a CEM as a tool, this study is also designed to explore the relative roles of thermal destabilization and moisture convergence in forcing convection and in changing the thermodynamic structure of the atmosphere.

## 2. Numerical simulations

The two-dimensional ( $x$  and  $z$ ) UCLA CEM (Krueger 1988) is used in this study. The details of the model have been described in earlier studies (e.g., Krueger 1988; Xu and Krueger 1991; Xu et al. 1992; Xu and Randall 1995b, 1996). Briefly, the CEM is based on the anelastic system of dynamical equations with the Coriolis acceleration. It includes physical parameterizations of 1) a third-moment turbulence closure (Krueger 1988), 2) a three-phase bulk cloud microphysics (Lin et al. 1983; Lord et al. 1984; Krueger et al. 1995), and 3) an interactive radiative transfer (Harshvardhan et al. 1987; Xu and Randall 1995a).

To achieve the objectives outlined in section 1, three idealized simulations were performed in this study. The designs of three simulations, Ctrl, McT, and TcM, are iden-

tical except for ways of prescribing large-scale advective cooling and moistening effects in each simulation. In the control simulation, Ctrl, both large-scale advective cooling and moistening effects, identical to the GATE Phase III means, are assumed to vary periodically with time ( $t$ ), according to the following function:

$$f(t) = [1 - \cos(2\pi t/T)]/2, \quad (1)$$

where  $T$  is the period of the time variation. This is chosen to be 27 h, as in Xu et al. (1992) and Xu and Randall (1995b). This period was chosen to avoid the diurnal cycle. Ctrl is identical to simulation I04 in Xu and Randall (1995b), which was used to examine cloud–radiation interaction mechanisms, except for a slightly different microphysics parameterization. That is, the final version of the modifications by Krueger et al. (1995) was not used in Xu and Randall (1995b) but is used in the present study. The results of Ctrl (see section 3) and I04 are, however, extremely similar.

In sensitivity simulations McT and TcM, only one type of large-scale advective effects is allowed to vary with time. The other component is assumed to be time invariant. The magnitude of the time-invariant advective cooling/moistening is half of the maximum value or time mean value over a 27-h cycle used in Ctrl. More specifically, McT is identical to Ctrl except for using time-invariant large-scale advective cooling, while TcM is identical to Ctrl except for using time-invariant large-scale moistening. In all simulations, the large-scale advective effects are imposed on the model grid points, uniformly in  $x$ .

The remaining aspects of the simulations are identical to those described in earlier studies with the UCLA CEM, especially simulation I04 in Xu and Randall (1995b). Only interactive longwave radiative transfer is used in all simulations described above so that the dominant periodic variation of the simulated cumulus ensembles is due to the externally imposed large-scale advective effects. There is no shear in the imposed geostrophic wind profile, which is used to prescribe the  $y$  component of the pressure gradient. It should be noted that the  $x$ -component wind profile does not change much with time except for small variations associated with the inertial oscillations. As in Xu et al. (1992), the Coriolis parameter for 15°N is used in all simulations. Each simulation was run for 19 days of physical time with a time step of 10 s. The domain size is 512 km, with a horizontal grid size of 2 km. Periodic lateral boundary conditions are used. The vertical coordinate is stretched to give finer resolution near the surface, with 33 layers. The underlying surface is an ocean with a fixed sea surface temperature of 299.9 K.

### 3. Results

#### *a. Time evolution of thermodynamic fields*

Figure 1a shows the time evolution of domain-averaged precipitable water for all three simulations de-

scribed in section 2. A 1-h average is applied to all variables from data saved every 5 min except for those variables shown without being taken an ensemble average (described later). A 3-h average is used to give a smoother time series plot. As shown in Fig. 1a, the precipitable water in the control simulation decreases gradually in the first five days and then oscillates around 47 kg m<sup>-2</sup>, which is 5 kg m<sup>-2</sup> lower than in the initial state. The column temperature undergoes a similar evolution (Fig. 1b), with an average value of 260.4 K for the last nine days, which is also slightly lower than the initial value of 261.1 K. The lower precipitable water and column temperature are related to the absence of solar radiation. Without solar radiation, the column temperature is lower, that is, more unstable, which increases the intensity of cumulus convection. More precipitable water is converted to precipitation as a result of stronger convection.

The time evolution of precipitable water and column temperature in McT and TcM (Fig. 1) is extremely similar to that in Ctrl. A noticeable feature is that the fluctuations around the mean values (dashed-dotted lines in Fig. 1) are almost out of phase between McT and TcM. The magnitudes of these fluctuations are approximately 1.5 kg m<sup>-2</sup> and 0.5 K. This can be more clearly seen from the temporal evolution of their ensemble mean deviations from the 19-day means (Fig. 2).

The ensemble average is defined with respect to the phase of large-scale advective forcing (Xu et al. 1992). Even though one component of the advective forcing does not change with time in the sensitivity simulations, the large-scale forcing in terms of the generalized CAPE (GCAPE) production (Wang and Randall 1994) indeed follows the phase of the time-varying component of the advective forcing (Fig. 3). The GCAPE production shown in Fig. 3 includes contributions from the radiative cooling and the surface turbulent fluxes, in addition to the imposed large-scale advective forcing. Data from the first 13 h of each simulation are excluded in all ensemble-averaged variables, due to the initial adjustment (see Fig. 1).

The most interesting result shown in Fig. 2 is that the temporal variations of the precipitable water and column temperature in Ctrl are almost out of phase with each other. The amplitudes of the variations are much smaller than those in the sensitivity simulations. These results can be explained with the column dry static energy  $\langle \bar{s} \rangle$  and moisture  $\langle \bar{q} \rangle$  budgets:

$$\left\langle \frac{\partial \bar{s}}{\partial t} \right\rangle = \left\langle \left( \frac{\partial \bar{s}}{\partial t} \right)_{1s} \right\rangle + \langle Q_R \rangle + H_s + LP, \quad (2)$$

$$L \left\langle \frac{\partial \bar{q}}{\partial t} \right\rangle = L \left\langle \left( \frac{\partial \bar{q}}{\partial t} \right)_{1s} \right\rangle - LP + LE, \quad (3)$$

where the angle brackets denote the vertical mass integrals from the bottom to the top of the atmosphere,

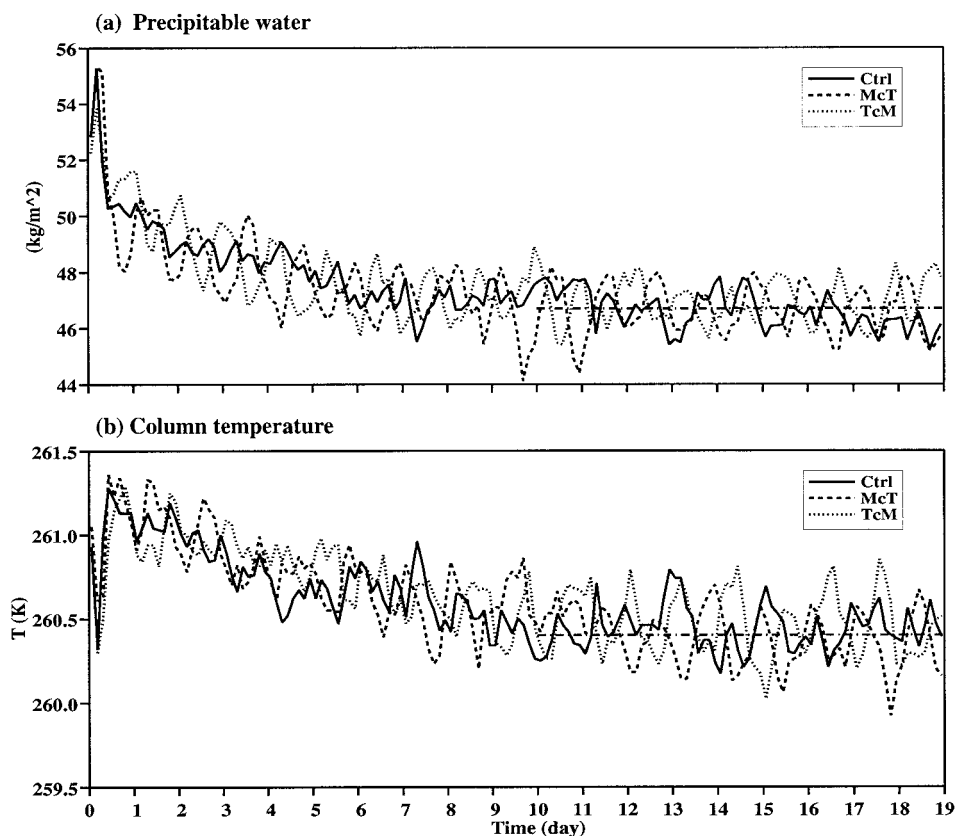


FIG. 1. Time sequence of the domain-averaged (a) precipitable water and (b) column temperature for simulations Ctrl, McT, and TcM. The horizontal dashed-dotted lines indicate the averaged value over the last nine days of the simulations.

$Q_R$  is the radiative heating rate,  $E$  is the surface evaporation rate,  $P$  is the surface precipitation rate,  $H_s$  is the surface sensible heat flux, and  $L$  is the latent heat of vaporization. The subscript “ls” denotes the large-scale advective effects. In Ctrl, the negative correlation between column temperature and precipitable water is related to the temporal fluctuations of  $P$  around its perfectly balanced values because of the temporal coherence of the imposed advective cooling and moistening effects. In McT and TcM, the large-scale advective cooling and moistening effects are not temporally coherent; one of them is time invariant. Thus, the time-change rates of column temperature and precipitable water have to be larger than in Ctrl in order to satisfy the budget requirements.

As mentioned earlier, the temporal evolution of the precipitable water (column temperature) in McT is out of phase with that in TcM, which can also be explained by the budget requirements. However, in either McT or TcM, the temporal evolution of column temperature is almost in phase with that of precipitable water except for small phase shifts. The phase difference suggests a weakly negative correlation between column temperature and precipitable water. The negative correlations in all simulations can be more clearly seen from scatter

diagrams of the deviations without the ensemble averaging (not shown), in agreement with the TOGA COARE observations (not shown).

Nevertheless, the surface precipitation rates respond to the imposed large-scale advective forcing similarly among the simulations (Fig. 4). [Note that the time series of the variables shown in Fig. 4 is smoothed using the adjacent values with a weighting function of (0.25, 0.5, 0.25) before taking an ensemble average. No smoothing is applied to any other variable.] The differences among the simulations are generally subtle though not negligible. The surface precipitation rate in Ctrl shows a strong modulation of cumulus convection by imposed large-scale advective forcing, with a single peak occurring between 13 and 14 h (Fig. 4a). Note that the large-scale advective forcing varies sinusoidally from zero at 0 h to maximum at 13.5 h and then to zero at 27 h (see Fig. 3). The major peaks in TcM and McT also occur later than in Ctrl, at 15 and 17 h, respectively, suggesting that cumulus convection responds to changes in thermal destabilization more quickly than to those in moisture convergence. This will be further examined in section 3c. On the other hand, the surface evaporation rates (Fig. 4b) are not strongly modulated by the imposed large-scale forcing and are similar among the simulations.

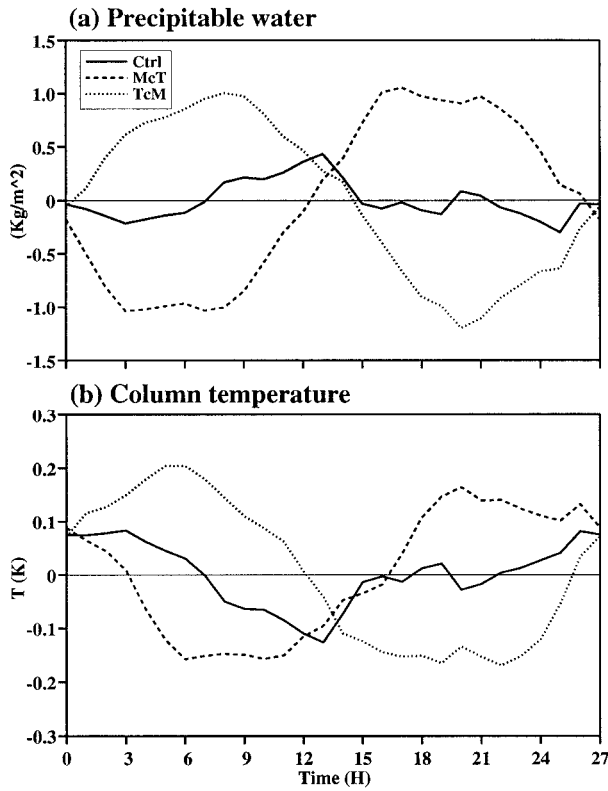


FIG. 2. Time sequence of the ensemble means of (a) precipitable water and (b) column temperature deviations for Ctrl, McT, and TeM. The abscissa is the phase of the imposed, time-varying large-scale advective process.

In summary, the simulated precipitable water and column temperature from the three simulations exhibit rather strong similarity on the long-term behavior but exhibit less similarity on the short-term behavior, due to the different short-term variations of the imposed large-scale advective forcing. Therefore, these three simulations can be regarded as one physical system with different short-term variations.

*b. Quasi-equilibrium behavior of simulated cumulus convection*

It should be emphasized here that the GCAPE tendency is about one order of magnitude smaller than the GCAPE production in all simulations (Fig. 3). The latter is equivalent to the large-scale forcing defined by Arakawa and Schubert (1974). Thus, the quasi-equilibrium assumption is well justified, based on the results shown in Fig. 3. On the other hand, the GCAPE production varies little as the imposed large-scale moistening effect varies. This suggests that the GCAPE production is largely contributed by thermal destabilization rather than moisture convergence. This is consistent with Xu and Arakawa (1992), in which the cloud work function (CWF: Arakawa and Schubert 1974) was used to calculate the large-scale forcing.

The same behavior can be directly examined from the CWF quasi equilibrium between large-scale and moist-convective processes (Arakawa and Schubert 1974; Arakawa and Chen 1987). For a cloud type with zero entrainment, the CWF quasi equilibrium can be expressed as a negative correlation between the surface relative humidity ( $RH_s$ ) and the lapse rate difference from moist adiabat ( $\Gamma - \Gamma_m$ ), for a fixed surface air temperature and cloud base height. A detailed description and discussion of this relationship can be found in Arakawa and Chen (1987).

Figure 5 shows scatterplots of  $RH_s$  versus the lapse rate ( $\Gamma$ ) between the surface and the 5.5-km level for data averaged over the entire domain in space and over

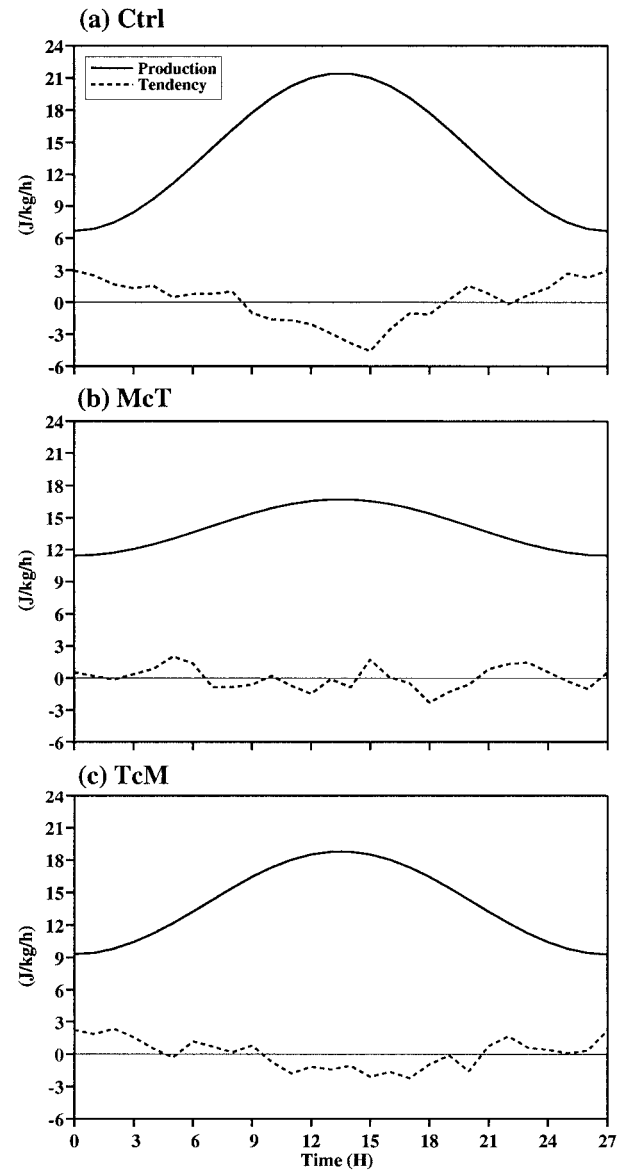


FIG. 3. As in Fig. 2 except for the generalized convective available potential energy production and tendency for Ctrl, McT, and TeM.

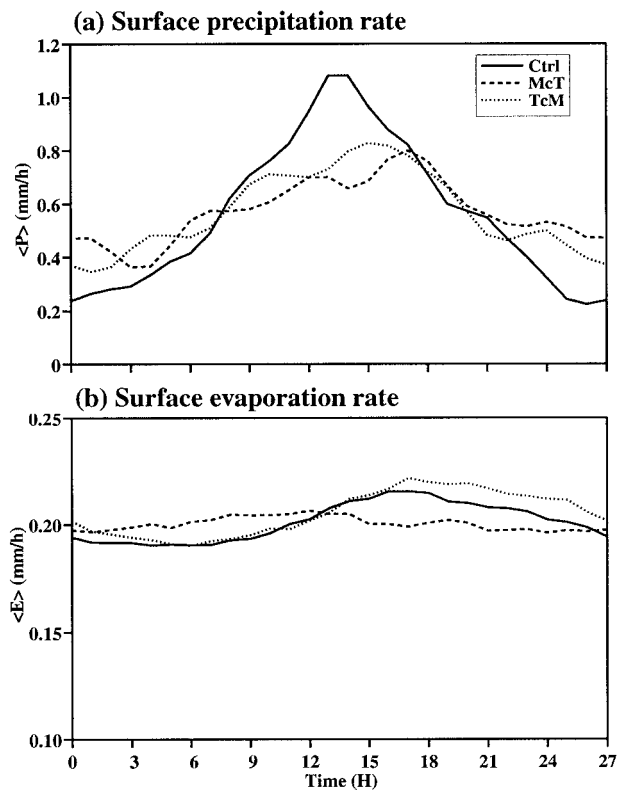


FIG. 4. As in Fig. 2 except for (a) surface precipitation rate and (b) surface evaporation rate for simulations Ctrl, McT, and TcM.

1 h in time. Observations from the TOGA COARE (Lin and Johnson 1996) are also shown. A negative correlation between  $RH_s$  and  $\Gamma$  exists in all simulations, indicating the existence of the CWF quasi equilibrium. This is consistent with earlier studies using the same CEM (Xu 1994) and with observations (Arakawa and Chen 1987), as well as with the TOGA COARE observations (Fig. 5d). The differences among Ctrl, McT, and TcM are rather small except for slightly less scatter in McT. The crowded clusters in Ctrl, McT, and TcM are related to small variations of  $RH_s$  as a result of a fixed SST in the simulations while  $\Gamma$  changes with the intensity of cumulus convection. During TOGA COARE,  $RH_s$  varies greatly with time due to greater fluctuations of SST and surface evaporation.

Results from two additional simulations not described in this study are most interesting (Figs. 5b and 5c). Simulation vM is identical to McT except for assuming zero large-scale advective cooling, while vT identical to TcM except for not allowing any large-scale moistening. Both vM and vT represent unrealistic situations where only one component of the large-scale advective forcing exists. Nevertheless, Figs. 5b and 5c show that simulations vT and vM occupy very different subdomains in the  $RH_s$  versus  $\Gamma$  diagram, compared to Ctrl, McT, and TcM. Most quasi-equilibrium states in vM are very humid near the surface and very stable in the lower troposphere, which

are beyond the subdomain occupied by the TOGA COARE observations (compare Figs. 5b with 5d). Most quasi-equilibrium states in vT are, however, very dry near the surface and very unstable in the lower troposphere, which are near the lower right portion of the subdomain occupied by the TOGA COARE observations.

In summary, the quasi-equilibrium states of simulated cumulus convection do not deviate much from the initial state when both large-scale advective cooling and moistening effects are imposed. That is, the deviations are small compared with observed variations of tropical oceanic convection. If large-scale advective cooling is imposed alone, the simulated quasi-equilibrium states tend to evolve into much more unstable and drier ones. They tend to evolve into much more moist and stable ones when only large-scale advective moistening is imposed. Although the latter two systems are not physically existing in the atmosphere, these results suggest that the variations of the lapse rates in the lower troposphere are strongly coupled to those of the surface moisture in the quasi-equilibrium states.

### c. Thermodynamic structures and their relationship to GCAPE variations

Figure 6 shows the ensemble means of potential temperature deviations ( $\theta'$ ) from the 19-day mean profiles for all three simulations. The maximum  $\theta'$  in Ctrl is approximately  $\pm 0.3$  K (Fig. 6a). The largest negative deviation occurs in the middle troposphere at 9 h. The negative deviation descends gradually to the lower troposphere. Such a phase propagation also appears in the positive deviation with its maximum appearing in the middle troposphere at 19 h. This type of phase shift between the lower and upper troposphere indicates a small temporal change of the lapse rate, that is, more unstable before maximum precipitation (Fig. 4) and more stable afterward between the surface and 9 km.

The patterns of  $\theta'$  in McT (Fig. 6b) are similar to those in Ctrl except for (i) larger magnitudes ( $\pm 0.5$  K), (ii) the lack of vertical phase propagations, and (iii) the location of maximum deviations. On the other hand, TcM shows  $\theta'$  almost opposite in signs, compared with Ctrl and McT, except for a phase shift of a few hours (Fig. 6c). The maximum deviations in TcM are located at lower levels and appear at earlier times.

The patterns of the relative (to the mean water vapor at each level of the respective simulation) deviations of water vapor mixing ratio ( $q'_w$ ) are shown in Fig. 7. They are rather similar to those of  $\theta'$  shown in Fig. 6 except for 1) the 3–6-h phase differences and 2) the different locations of the maximum deviations. A noticeable difference between the control and sensitivity simulations is that the deviations have opposite signs in the lowest 1 km and the thick layer above in Ctrl but not in McT and TcM.

The results shown in Figs. 6 and 7 can be simply stated as follows. The temporal variation of the large-scale moistening effects is largely responsible for the

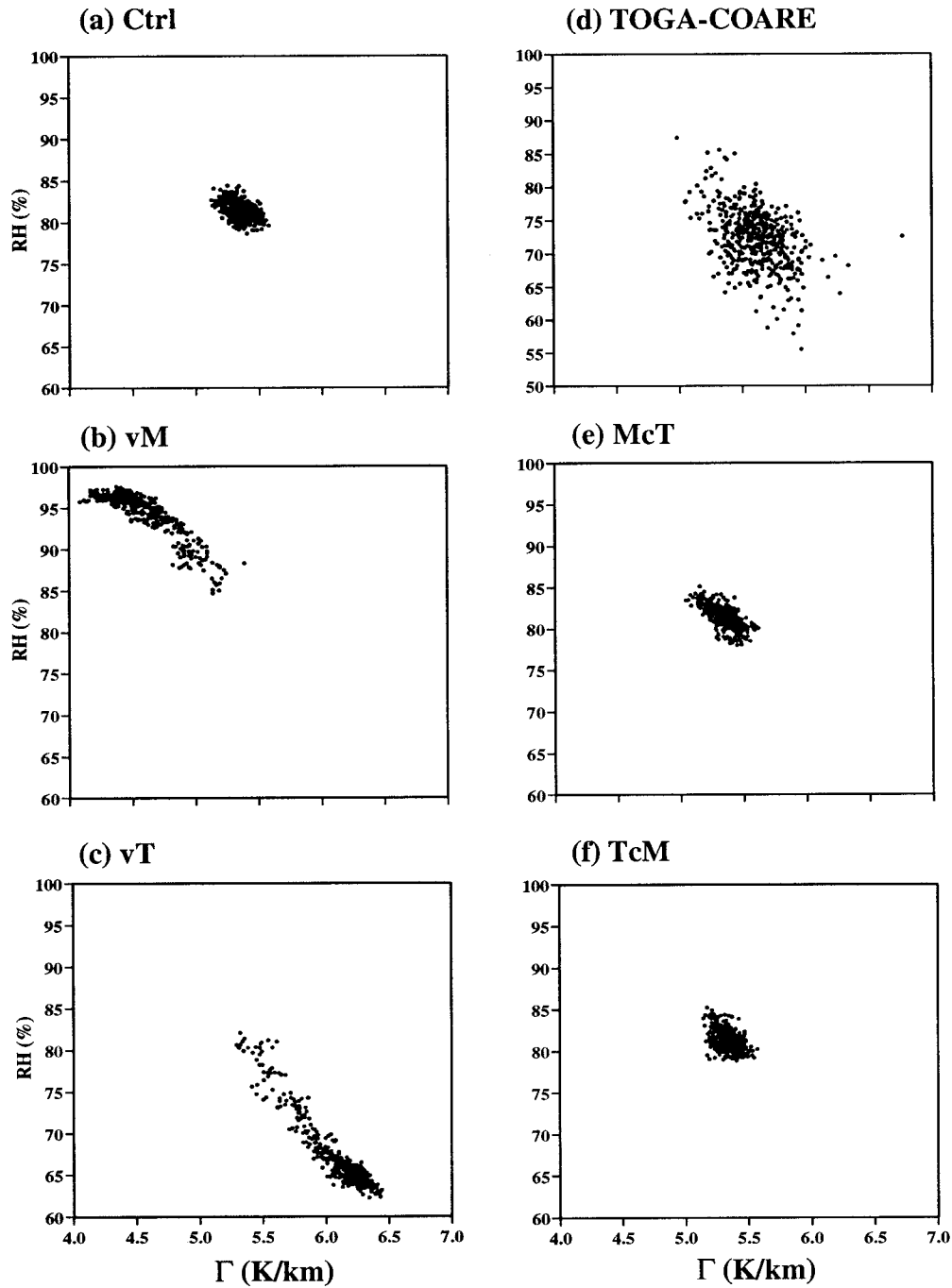


FIG. 5. Scatterplots of the surface relative humidity vs the lapse rate for five simulations and TOGA COARE observations. Simulations vM and vT are not described in this study.

simulated temporal variations of the thermodynamic structures in the control simulation, while that of the large-scale cooling effects plays a less significant role above the lower troposphere.

Next, the ensemble means of the GCAPE are shown (solid lines in Fig. 8). Unlike conventional measures of CAPE, the GCAPE includes the effects of multiple parcels originating at multiple levels and effects of com-

pensating motions in the environment (Lorenz 1978, 1979; Randall and Wang 1992; Wang and Randall 1994). A striking feature in Fig. 8 is that the GCAPE is larger than the 19-day mean (dashed lines) before the large-scale forcing, as measured by the GCAPE production (Fig. 3), reaches its maximum at 13.5 h but smaller thereafter. This is expected because there is a phase delay between the intensity of cumulus convec-

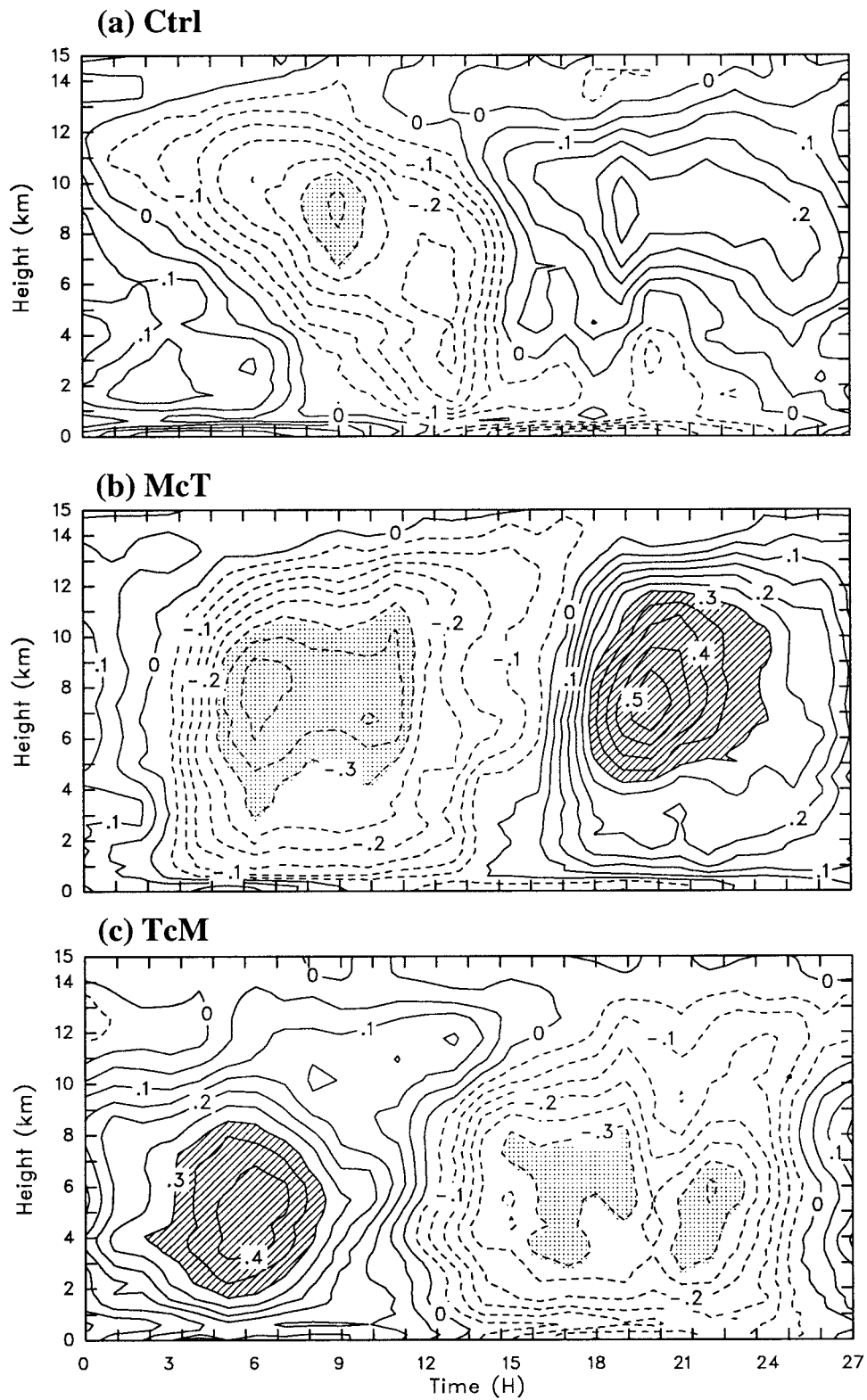


FIG. 6. Time-height cross section of the ensemble mean of potential temperature deviation for Ctrl, McT, and TcM. The contour interval is 0.05 K. Contours over 0.3 K are hatched. Contours less than -0.3 K are dotted. The abscissa is the phase of the imposed, time-varying large-scale advective process.

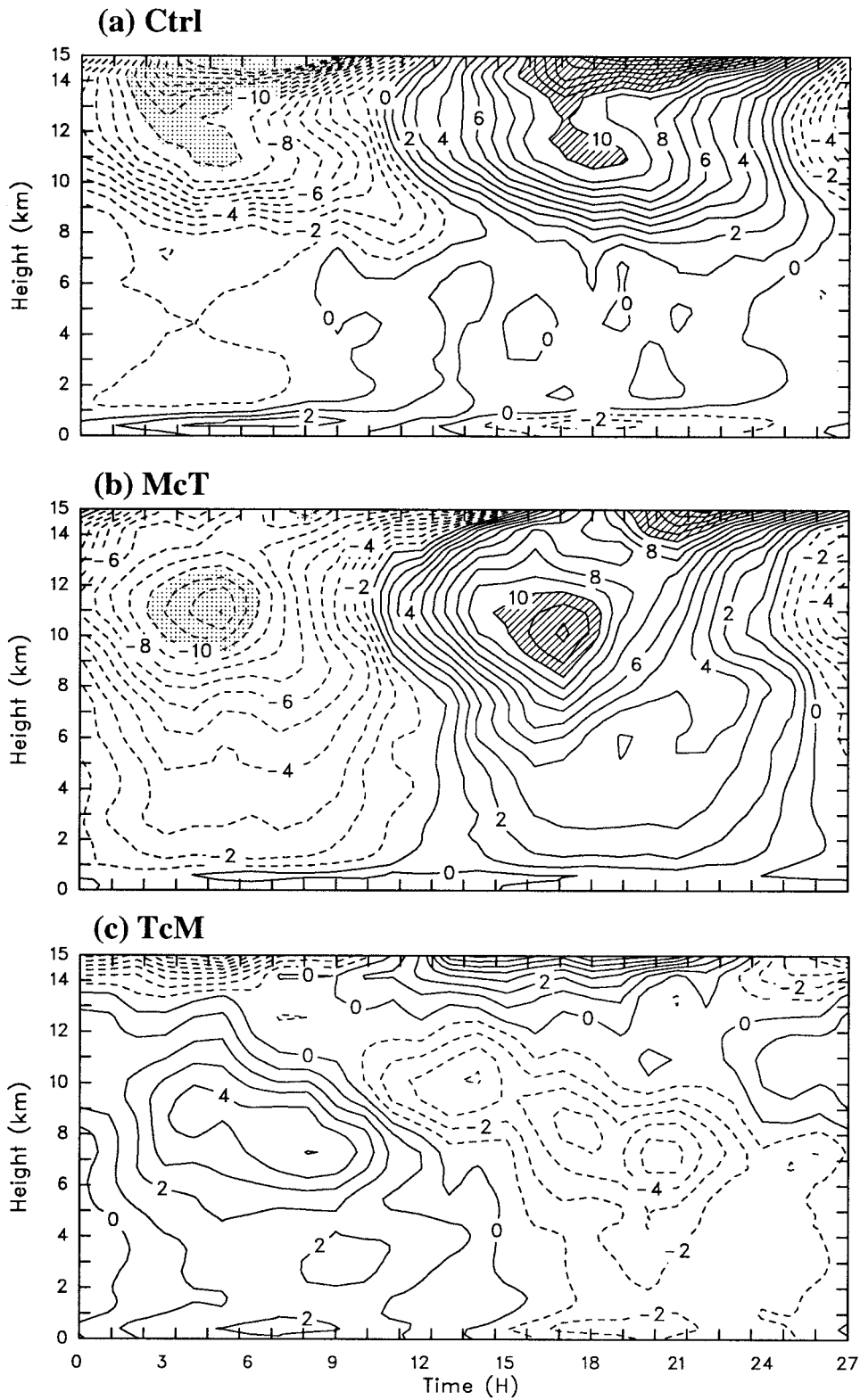


FIG. 7. As in Fig. 6 except for the ensemble mean of the relative deviation of water vapor mixing ratio (with respect to the mean value at each level of the respective simulation). The contour interval is 1%. Contours over 10% are hatched. Contours less than -10% are dotted.

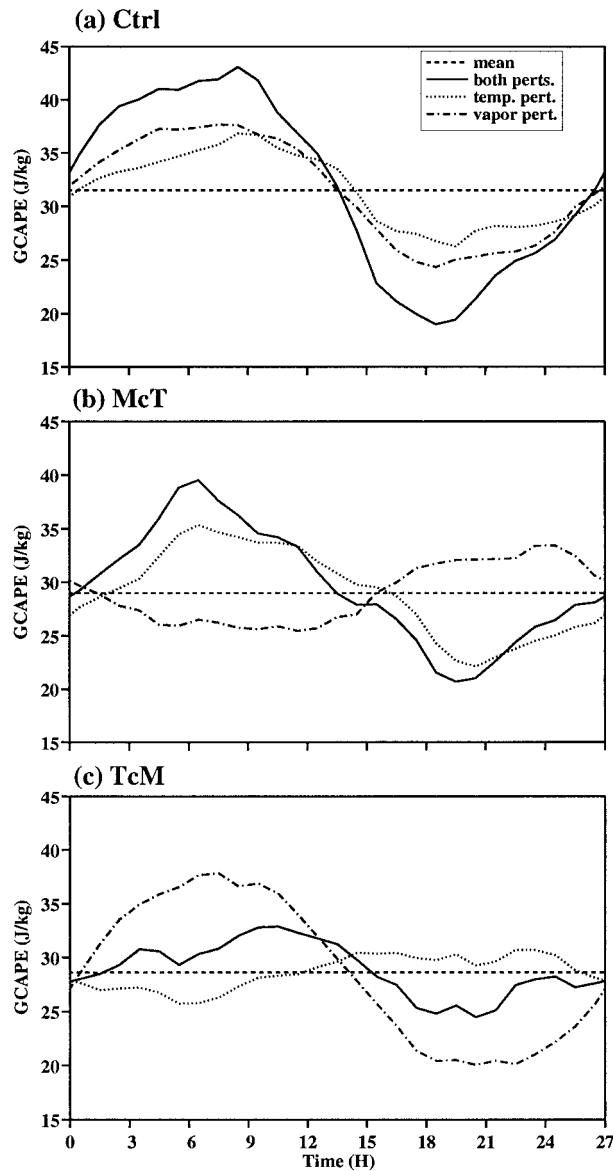


FIG. 8. As in Fig. 2 except for GCAPE of the mean states, GCAPE with both temperature and water vapor mixing ratio deviations, GCAPE with temperature deviation only, and GCAPE with water vapor mixing ratio deviation only.

tion and the imposed large-scale advective forcing (Xu et al. 1992) such that GCAPE is accumulated before the peak intensity of cumulus convection and consumed afterwards.

The GCAPE temporal variations are discussed below to understand the higher-order behavior of quasi-equilibrium cumulus ensembles, which also includes their relationships with the thermodynamic structures and with the imposed large-scale advective cooling and/or moistening effects.

Figure 8 shows that the amplitude of the GCAPE variations in Ctrl is greater than that in the sensitivity simulations. For example, the GCAPE variations in TcM

are very small during the 27-h cycle. This result suggests that the temporal coherence of large-scale advective cooling and moistening (e.g., by large-scale vertical motion) increases/decreases the GCAPE values more than when incoherent forcings (e.g., horizontal advection) are imposed. A simple explanation is that contributions of  $\theta'$  and  $q'_v$  to GCAPE variations are in phase with each other in Ctrl (Fig. 8a) but they are not necessarily so in the sensitivity tests (Figs. 8b, c).

Another difference between the control and sensitivity simulations is in the timing of the maximum and minimum GCAPE values. For example, the maximum and minimum GCAPE in TcM occur about 3 h later than those in Ctrl. This phase difference is similar to that in the surface precipitation rate (Fig. 4).

Figure 8 also shows the ensemble means of GCAPE values calculated with  $\theta'$  (Fig. 6) only and with  $q'_v$  (Fig. 7) only. Before comparing the GCAPE variations due to  $\theta'$  and  $q'_v$  in each simulation, one should notice that GCAPE deviations are nonlinear functions of  $\theta'$  and  $q'_v$ . In Ctrl, both  $\theta'$  and  $q'_v$  contribute to the GCAPE temporal variations similarly, as in the total GCAPE variations (solid line in Fig. 8a). This can be explained by the vertical structures of both  $\theta'$  and  $q'_v$ . The GCAPE deviation from the 19-day mean is positive (negative) when the lower-to-middle troposphere (Fig. 6a) is more unstable (stable). The more humid surface layer (rising parcels) and the drier middle-to-upper troposphere (sinking parcels) favor positive GCAPE deviations while the drier surface layer and the more moist middle-to-upper troposphere produce negative GCAPE deviations (Fig. 7a).

In the sensitivity simulations, the GCAPE temporal variations due to  $\theta'$  only and  $q'_v$  only are not similar at all. In fact, the deviations from the 19-day means are opposite in signs. The GCAPE temporal variations due to  $\theta'$  only in McT ( $q'_v$  only in TcM) somewhat dominate the total GCAPE variations, while those due to  $q'_v$  only ( $\theta'$  only) counterbalance the dominance (Figs. 8b and 8c). These results can also be explained by the thermodynamic structures. The lapse rate and its temporal variation in McT are similar to those in Ctrl, while those in TcM are opposite to Ctrl (Fig. 6). Thus, the contributions of  $\theta'$  to the GCAPE deviations are opposite in signs between McT and TcM. In spite of the similarity of the overall structures of  $q'_v$  between Ctrl and McT (Fig. 7), the GCAPE deviations due to  $q'_v$  only are opposite in signs between Ctrl and McT. This is largely related to the  $q'_v$  difference in the thin layer below 1 km. On the other hand, the  $q'_v$  contribution to the GCAPE deviations in TcM is far more dominant than in either Ctrl or McT, due to the thick moister (drier) layer in the lower troposphere. Note that the absolute water vapor deviations should be used in the above discussion, instead of the relative deviations shown in Fig. 7.

In the aforementioned results, a surprising finding is that  $\theta'$  is the dominant contributor to the GCAPE variations when time-varying advective moistening is im-

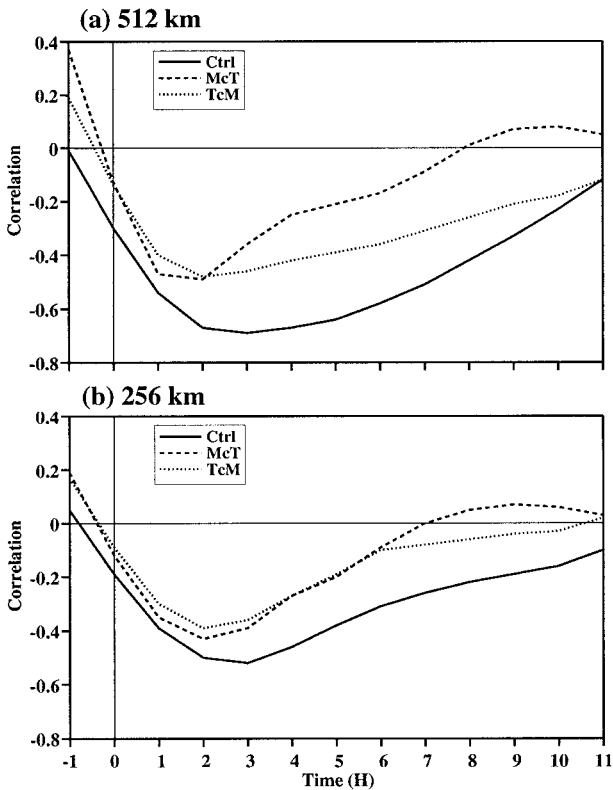


FIG. 9. Lag correlation coefficients between GCAPE and the surface precipitation rate for (a) the 512-km averaging and (b) the 256-km averaging of all three simulations.

posed, while  $q'_v$  is the dominant one when time-varying advective cooling is imposed.

#### d. Relationship between GCAPE and the intensity of cumulus convection

As mentioned in section 1, observations show that there is a negative correlation between CAPE (GCAPE) and the intensity of cumulus convection (Thompson et al. 1979; Wang and Randall 1994). Explicit cumulus ensemble simulations with observed large-scale data also confirm such a relationship (Xu and Randall 1996). Because of the coarse temporal resolutions of the observational datasets, the exact nature of such a relationship in terms of lag correlation cannot be quantified.

Figures 9a and 9b show lag correlations between GCAPE and the surface precipitation rate for all three simulations, using data averaged over the entire domain (512 km) and half domain (256 km), respectively. The lag time from  $-1$  to  $+11$  h is chosen. A *positive* lag time indicates that the GCAPE precedes the surface precipitation rate. The maximum lag is defined when the absolute value of negative correlation is the largest. Statistically, this maximum lag measures the time interval between the maximum surface precipitation rate and the minimum GCAPE, which is the timescale for GCAPE to be consumed to its lowest value after the peak pre-

cipitation occurs. It can also be understood as the time-scale for GCAPE to accumulate to its highest value after cumulus convection reaches its lowest intensity (i.e., the minimum surface precipitation rate). Thus, the maximum lag is similar to the adjustment timescale defined by Arakawa and Schubert (1974) except without putting a restriction on the absence of large-scale forcing.

As seen from Fig. 9a, the negative correlation at zero lag appears for every simulation (from  $-0.10$  to  $-0.28$ ), which agrees with observations. The absolute value of the negative correlation at zero lag for the 512-km averaging ( $-0.28$ ) is the largest in Ctrl, which is also the case for any lags between  $-1$  and  $11$  h. This result is apparent by comparing the results shown in Figs. 4a and 8. For the 512-km averaging, the maximum lag is 3 h in Ctrl and 2 h in both McT and TcM. Results from the 256-km averaging (Fig. 9b) are similar to those for the 512-km averaging except for 1) the smaller differences among the simulations and 2) the smaller negative correlations in all simulations. A possible explanation for these differences between 512- and 256-km averagings is that cumulus ensembles for 256-km subdomains are weakly controlled by the imposed large-scale advective forcing.

The comparison between Figs. 9a and 9b apparently suggests that the lag correlation is somewhat dependent upon the horizontal averaging distance. To further demonstrate this, Fig. 10a shows the lag correlation for averagings between 512 and 32 km of Ctrl. It can be readily seen from Fig. 10a that the absolute magnitude of lag correlations for all lags decreases and the maximum lag becomes shorter as the horizontal averaging distance decreases. For instance, the maximum lag is only 1 h for the 32-km averaging. Such a dependence suggests that the CWF quasi equilibrium becomes a more accurate approximation as the horizontal averaging distance decreases. This is consistent with the conclusion obtained from semiprognostic tests of the Arakawa-Schubert cumulus parameterization by Xu and Arakawa (1992). On the other hand, the small lags for smaller subdomain sizes may also be related to the fact that “large-scale” and convective-scale processes become less separable as subdomain sizes decrease.

Figure 10b shows a similar diagram as Fig. 10a except for GATE simulation and observations. The details of the GATE simulation with observed large-scale forcing and SST are described by Xu and Randall (1996). The lag correlation for averagings between 64 and 512 km from the simulation is generally similar to that from the observational data, although the latter does not show much variation for large lags due to temporal smoothing of the sounding data (Thompson et al. 1979). The difference between simulation and observations can be partially attributed to the coarse temporal resolution of the observational data (3 h). Nevertheless, Fig. 10b shows a similar dependency of the lag correlation on the horizontal averaging distance as in Ctrl (Fig. 10a).

The comparison between GATE simulation and the

three simulations presented in this study unambiguously points out the existence of 1) a negative lag correlation between the surface precipitation and the GCAPE and 2) the maximum lag of a few hours. Additional supporting evidence is shown in Fig. 11. The results shown in Fig. 11a are obtained from two simulations with diurnally varying radiation. The imposed large-scale advective moistening and cooling are time invariant. The “no shear” simulation is identical to I05 presented in Xu and Randall (1995b) while the “shear” simulation uses a geostrophic wind profile identical to that in Q02 of Xu et al. (1992). The remaining aspects of these two simulations are identical. The lag correlation for the 256-km averaging from the two simulations is similar to Ctrl (Fig. 9b). The shear simulation shows slightly larger lag correlation at large lags. Its maximum lag is 3 h, compared to 2-h maximum lag in the no-shear simulation.

The results presented in Fig. 11b are based on simulations similar to those of Sui et al. (1994), in which an observed large-scale vertical velocity profile from the Marshall Islands (Yanai et al. 1973) is imposed to the model grid points. The details of the simulations will be published elsewhere. Simulation cW is identical to that in Sui et al. (1994) except with diurnally varying solar radiation. Simulation vhW allows the prescribed

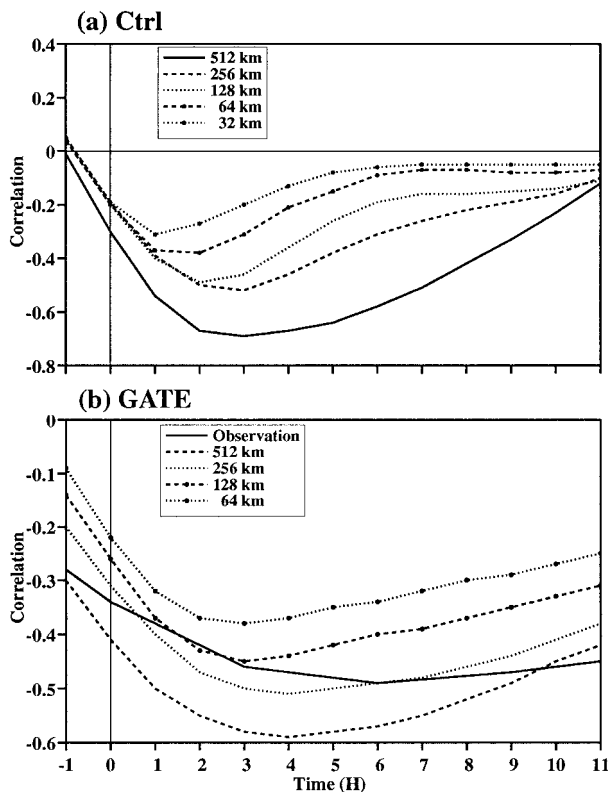


FIG. 10. Lag correlation coefficients between GCAPE and the surface precipitation rate as a function of horizontal averaging distances for (a) Ctrl and (b) GATE simulation and observation. Note the different scales in (a) and (b).

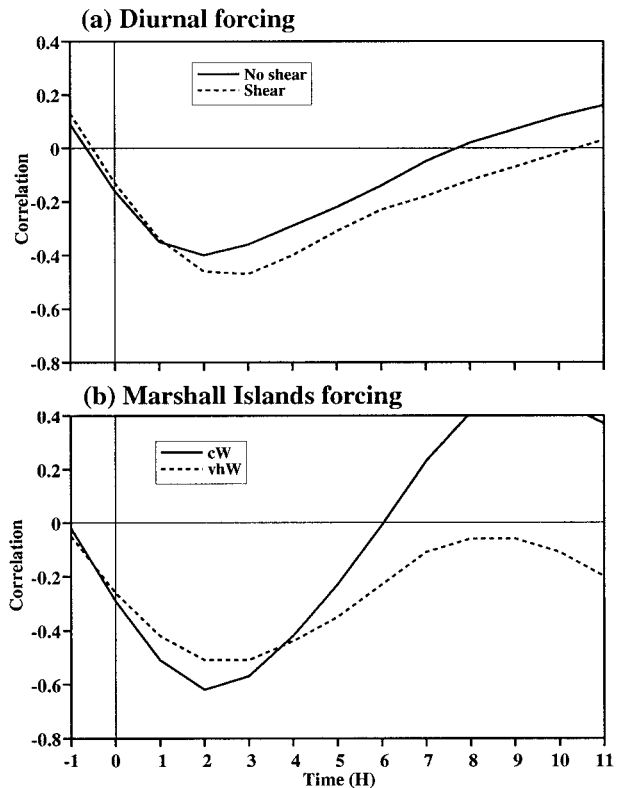


FIG. 11. As in Fig. 9b except for (a) diurnal forcing simulations and (b) Marshall Islands forcing simulations. See texts for further explanation.

large-scale vertical velocity vary sinusoidally with a period of 54 h. The result shown in Fig. 11b is similar to that in Ctrl for lags less than 6 h. The maximum lags in these two simulations are 2–3 h. Therefore, results from a range of simulations are largely similar to each other although the character and period of the imposed large-scale forcing are very different.

In summary, the maximum lag can be regarded as an independent, direct estimate of the adjustment timescale without involving with an idealized model (see Arakawa 1993). It can be interpreted as the adjustment timescale from disequilibrium to quasi-equilibrium states in the presence of time-varying large-scale forcing.

#### 4. Summary and discussion

In this study, several related aspects of the quasi-equilibrium behavior of explicitly simulated, tropical oceanic cumulus ensembles have been examined: 1) the relationship between the GCAPE variation and the thermodynamic structure, 2) the relative importance of large-scale thermal destabilization and moisture convergence in driving cumulus convection and in determining the higher-order behavior of cumulus ensembles, and 3) the adjustment timescale for quasi-equilibrium cumulus ensembles. Two sensitivity simulations have been performed by imposing time-varying/invariant

large-scale advective cooling effects and time invariant/varying large-scale advective moistening effects. The results have been compared with a control simulation performed with both large-scale advective cooling and moistening effects that are time varying. Results from additional simulations under very different large-scale conditions have also been used to examine the last aspect.

The temporal variations of the simulated precipitable water and column temperature from the three simulations exhibit rather strong similarity on the long-term behavior but exhibit less similarity on the short-term behavior due to the different short-term variations of the imposed large-scale forcing. High-frequency fluctuations of column temperature and precipitable water are negatively correlated, especially in the control simulation. The existence of quasi-equilibrium between large-scale and convective-scale processes is confirmed by (i) that the GCAPE tendency is about one order of magnitude smaller than the GCAPE production and (ii) that the variations of the lapse rates in the lower troposphere are strongly coupled to those of the surface moisture. It is found that the GCAPE production is largely contributed by thermal destabilization rather than moisture convergence. Both large-scale processes strongly modulate cumulus convection but convection responds to changes in thermal destabilization more quickly than to those in moisture convergence.

In spite of the small GCAPE tendency, the GCAPE temporal variations are highly related to the intensity of cumulus convection. The GCAPE is accumulated before the peak intensity of cumulus convection and consumed afterward. Such GCAPE variations are also related to the thermodynamic structure and the imposed large-scale forcing. In the control simulation, the GCAPE variations are nearly equally contributed by temperature and water vapor variations. When temporally incoherent large-scale cooling and moistening effects are imposed, the temporal variations of the intensity of cumulus convection are largely determined by the time-varying component of the forcing. This creates an imbalance of either the heat or moisture budget due to the strong coupling of cumulus drying and warming. Thus, temperature (water vapor) deviations are found to be the dominant contributors to the GCAPE temporal variations when the imposed advective cooling (moistening) is time invariant, but the water vapor (temperature) deviations contribute to the GCAPE deviations in opposite signs with smaller magnitudes. Therefore, the temporal incoherence of large-scale thermal destabilization and moisture convergence influences the higher-order behavior of quasi-equilibrium cumulus ensembles.

A significant finding of the present study is the existence of (i) a negative lag correlation between the surface precipitation rate and the GCAPE and (ii) the maximum lag of a few hours, under different character and period of the imposed large-scale forcing. The maximum lag is 2–3 h in the three simulations examined in

this study. Additional simulations with idealized forcings or with observed large-scale forcings give an estimate of the maximum lag between 1 and 5 h. It is further found that the negative lag correlation becomes smaller and the maximum lag becomes shorter as the horizontal averaging distance decreases.

In this study, the maximum lag is interpreted as the adjustment timescale, which represents the adjustment time from disequilibrium to quasi-equilibrium states in the presence of time-varying large-scale forcing. This study provides a direct estimate of the adjustment timescale for the first time without invoking an idealized model. Statistically, the maximum lag measures the time interval between the maximum surface precipitation rate and the minimum GCAPE or that between the minimum surface precipitation rate and the maximum GCAPE. The traditional adjustment timescale measures the timescale for consumption of convective instability in the absence of large-scale forcing (Lord and Arakawa 1980). The understanding of the adjustment timescale provided by this study should be helpful for relaxing the quasi-equilibrium assumption and for further improving the prognostic approach in cumulus parameterization.

*Acknowledgments.* This research was supported by the Environmental Sciences Division of U.S. Department of Energy under Grant DE-FG03-95ER61968 as part of the Atmospheric Radiation Measurement Program. The computations were performed at the National Energy Research Supercomputer Center, Livermore, California.

#### REFERENCES

- Arakawa, A., 1969: Parameterization of cumulus clouds. *Proc. WMO/IUGG Symp. on Numerical Weather Prediction*, Tokyo, Japan, Japan Meteorology Agency, 1–6.
- , 1993: Closure assumptions in the cumulus parameterization problem. *The Representation of Cumulus Convection in Numerical Models of the Atmosphere*, K. A. Meteor. Monogr., No. 46, 1–16.
- , and W. H. Schubert, 1974: Interaction of a cumulus cloud ensemble with the large-scale environment, Part I. *J. Atmos. Sci.*, **31**, 674–701.
- , and J.-M. Chen, 1987: Closure assumptions in the cumulus parameterization problem. *Short- and Medium-Range Numerical Prediction, Collection of Papers at the WMO/IUGG NWP Symp.*, Tokyo, Japan, T. Matsuno, Ed., Meteor. Soc. Japan, 107–131.
- Betts, A. K., and M. J. Miller, 1986: A new convective adjustment scheme. Part II: Single column tests using GATE wave, BOMEX, ATEX and arctic air mass data sets. *Quart. J. Roy. Meteor. Soc.*, **112**, 692–709.
- Charney, J. G., and A. Eliassen, 1964: On the growth of the hurricane depression. *J. Atmos. Sci.*, **21**, 68–75.
- Cheng, M.-D., and M. Yanai, 1989: Effects of downdrafts and mesoscale convective organization on the heat and moisture budgets of tropical cloud clusters. Part III: Effects of mesoscale convective organization. *J. Atmos. Sci.*, **46**, 1566–1588.
- Emanuel, K. A., 1991: A scheme for representing cumulus convection in large-scale models. *J. Atmos. Sci.*, **48**, 2313–2335.
- Grell, G. A., Y.-H. Kuo, and R. J. Pasch, 1991: Semi-prognostic tests

- of cumulus parameterization schemes in the middle latitudes. *Mon. Wea. Rev.*, **119**, 5–31.
- Harshvardhan, R. Davies, D. A. Randall, and T. G. Corsetti, 1987: A fast radiation parameterization for general circulation models. *J. Geophys. Res.*, **92**, 1009–1016.
- Krueger, S. K., 1988: Numerical simulation of tropical cumulus clouds and their interaction with the subcloud layer. *J. Atmos. Sci.*, **45**, 2221–2250.
- , Q. Fu, K. N. Liou, and H.-N. Chin, 1995: Improvements of an ice-phase micro-physics parameterization for use in numerical simulations of tropical convection. *J. Appl. Meteor.*, **34**, 281–287.
- Kuettner, J. P., and D. E. Parker, 1976: GATE: Report on the field phase. *Bull. Amer. Meteor. Soc.*, **57**, 11–27.
- Kuo, H. L., 1965: On formation and intensification of tropical cyclones through latent heat release by cumulus convection. *J. Atmos. Sci.*, **22**, 40–63.
- , 1974: Further studies of the parameterization of the influence of cumulus convection on large-scale flow. *J. Atmos. Sci.*, **31**, 1232–1240.
- Lin, X., and R. H. Johnson, 1996: Kinematic and thermodynamic characteristics of the flow over the western Pacific warm pool during TOGA COARE. *J. Atmos. Sci.*, **53**, 695–715.
- Lin, Y.-L., R. D. Farley, and H. D. Orville, 1983: Bulk parameterization of the snow field in a cloud model. *J. Climate Appl. Meteor.*, **22**, 1065–1092.
- Lord, S. J., and A. Arakawa, 1980: Interaction of a cumulus cloud ensemble with the large-scale environment. Part II. *J. Atmos. Sci.*, **37**, 2677–2692.
- , H. E. Willoughby, and J. M. Piotrowicz, 1984: Role of a parameterized ice-phase microphysics in an axisymmetric, non-hydrologic tropical cyclone model. *J. Atmos. Sci.*, **41**, 2836–2848.
- Lorenz, E. N., 1978: Available energy and the maintenance of a moist circulation. *Tellus*, **30**, 15–31.
- , 1979: Numerical evaluation of moist available energy. *Tellus*, **31**, 230–235.
- Manabe, S., and R. F. Strickler, 1964: Thermal equilibrium of the atmosphere with a convective adjustment. *J. Atmos. Sci.*, **21**, 361–385.
- Moorthi, S., and M. J. Suarez, 1992: Relaxed Arakawa–Schubert: A parameterization of moist convection for general circulation models. *Mon. Wea. Rev.*, **120**, 978–1002.
- Randall, D. A., and J. Wang, 1992: The moist available energy of a conditionally unstable atmosphere. *J. Atmos. Sci.*, **49**, 240–255.
- , and D.-M. Pan, 1993: Implementation of the Arakawa–Schubert cumulus parameterization with a prognostic closure. *The Representation of Cumulus Convection in Numerical Models of the Atmosphere*, K. A. Emanuel and D. J. Raymond, Eds., *Meteor. Monogr.*, No. 46, 137–144.
- Raymond, D. J., 1995: Regulation of moist convection over the west Pacific warm pool. *J. Atmos. Sci.*, **52**, 3945–3959.
- Riehl, H., and J. S. Malkus, 1958: On the heat balance of the equatorial trough zone. *Geophysica (Helsinki)*, **6**, 503–538.
- Stevens, B., D. A. Randall, X. Lin, and M. T. Montgomery, 1997: A comment on “On large-scale circulations in convecting atmospheres by Emanuel, Neelin and Bretherton.” *Quart. J. Roy. Meteor. Soc.*, **123**, 1771–1778.
- Sui, C.-H., K.-M. Lau, W.-K. Tao, and J. Simpson, 1994: The tropical water and energy cycle in a cumulus ensemble model. Part I: Equilibrium climate. *J. Atmos. Sci.*, **51**, 711–728.
- Thompson, R. M., Jr., S. W. Payne, E. E. Recker, and R. J. Reed, 1979: Structure and properties of synoptic-scale wave disturbances in the intertropical convergence zone of the eastern Atlantic. *J. Atmos. Sci.*, **36**, 53–72.
- Wang, J., and D. A. Randall, 1994: The moist available energy of a conditionally unstable atmosphere. Part II: Further analysis of GATE data. *J. Atmos. Sci.*, **51**, 703–710.
- Webster, P. J., and R. Lukas, 1992: TOGA COARE: The Coupled Ocean–Atmosphere Response Experiment. *Bull. Amer. Meteor. Soc.*, **73**, 1377–1417.
- Williams, E. R., and N. Renno, 1993: An analysis of the conditional instability of the tropical atmosphere. *Mon. Wea. Rev.*, **121**, 21–36.
- Xu, K.-M., 1994: A statistical analysis of the dependency of closure assumptions in cumulus parameterization on the horizontal resolution. *J. Atmos. Sci.*, **51**, 3674–3691.
- , and S. K. Krueger, 1991: Evaluation of cloudiness parameterizations using a cumulus ensemble model. *Mon. Wea. Rev.*, **119**, 342–367.
- , and A. Arakawa, 1992: Semi-prognostic tests of the Arakawa–Schubert cumulus parameterization using simulated data. *J. Atmos. Sci.*, **49**, 2421–2436.
- , and D. A. Randall, 1995a: Impact of interactive radiative transfer on the macroscopic behavior of cumulus ensembles. Part I: Radiation parameterization and sensitivity tests. *J. Atmos. Sci.*, **52**, 785–799.
- , and —, 1995b: Impact of interactive radiative transfer transfer on the macroscopic behavior of cumulus ensembles. Part II: Mechanisms for cloud–radiation interactions. *J. Atmos. Sci.*, **52**, 800–817.
- , and —, 1996: Explicit simulation of cumulus ensembles with the GATE Phase III data: Comparison with observations. *J. Atmos. Sci.*, **53**, 3710–3736.
- , A. Arakawa, and S. K. Krueger 1992: The macroscopic behavior of cumulus ensembles simulated by a cumulus ensemble model. *J. Atmos. Sci.*, **49**, 2402–2420.
- Yanai, M., S. Esbensen, and J.-H. Chu, 1973: Determination of bulk properties of tropical cloud clusters from large-scale heat and moisture budgets. *J. Atmos. Sci.*, **30**, 611–627.